Absolute molecular flux and angular distribution measurements to characterize DNA / RNA vapor jets

J. Tabet[1], S. Eden[1,*], S. Feil[1], H. Abdoul-Carime[1], B. Farizon[1], M. Farizon[1], S. Ouaskit [2], T.D.Märk[**]

[1]*Université de Lyon, F-69003, Lyon, France; Université Lyon 1, Villeurbanne; CNRS/IN2P3, UMR5822, Institut de Physique Nucléaire de Lyon, 4 rue Enrico Fermi, Villeurbanne*

[2] *Laboratoire de physique de la matière condensée, Unité associée au CNRST (URAC 10), Faculté des sciences Ben M'sik, B.P.7955, Casablanca, Morocco*

Abstract

Vapor jets of DNA and RNA bases (adenine, cytosine, thymine, and uracil) from an oven with a capillary exit have been studied in the *intermediate* regime between molecular and viscous flow corresponding to Knudsen numbers in the range $0.1 < K_n < 10$. The temperature control method ensured stationary flow. Assuming the Knudsen hypothesis, the pressure of sublimated molecules in the oven was determined as a function of temperature and the transmission probability of the capillary (Clausing factor). Thus it was possible to relate the oven temperature and pressure to the total flux through the capillary, determined by measuring the total mass of DNA / RNA base molecules condensed on a cold surface intersecting the jet. The angular distribution of molecules in the jet has been also studied experimentally using an optical interference method. The measured profiles are in good agreement with Troïtskii's [Sov. Phys. JETP 7 (1962) 353] analytical law for $(\cos\theta)^{3/2}$ angular dependence in the intermediate regime with error functions associated with the mean free path between intermolecular collisions.

[*] Permanent addess : *Dept. Physics and Astronomy, The Open University (OU), Walton hall, Milton Keynes, MK76AA, UK*

[**] *Institut für Ionenphysik und Angewandte Physik, Leopold Franzens Universität, Technikerstrasse 25, A-6020 Innsbruck, Austria*

1. Introduction

The experimental study of biomolecular ionization can provide insights to further our understanding of radiation damage mechanisms in living material. Indeed a significant goal in radiobiology is to characterize the ionization events which can damage key biomolecules (e.g. DNA, RNA, and their constituents) [1]. This represents an important step towards an elucidation of the physical interactions which can initiate the sequences of chemical, biochemical, and cellular processes associated with harmful physiological effects. From this perspective, Monte Carlo track structure codes provide a valuable framework to study initial radiation damage mechanisms on the molecular scale [2]. Such programs require a complete set of cross sections for particle-biomolecule collisions in order to simulate localized energy deposition and the transport of *primary* (incident energetic species) and *secondary* particles (products of ionization and fragmentation events) in a representative cellular environment. However, absolute cross section measurements are rare for biomolecules which require heating (or another technique such as laser desorption or MALDI) to produce suitable gas-phase targets. The scarcity of reliable absolute cross sections for interactions with sublimated biomolecules is primarily due to the difficulty in determining the target *thickness* traversed by a projectile beam intersecting a vapor jet from an oven. This parameter depends on (*i*) the respective positions of the oven and the incident beam, (ii) the total flux of target molecules as a function of the oven temperature, and (*iii*) the angular distribution of molecules in the jet. Accordingly the present work provides new experimental measurements of the total flux and angular profiles of DNA and RNA base jets (adenine, cytosine, thymine, and uracil) from a Knudsen-type oven. Sublimation enthalpies calculated using the total flux measurements are in good agreement with the literature and the observed angular profiles are consistent with theoretical calculations based on the dimensions of the oven's capillary exit. The Lyon oven design has been used in a wide range of crossed-beam experiments on sublimated DNA / RNA bases [3-5] so the present jet characterization may be applied to normalize previous relative measurements. More generally, a full description is provided of the

procedure to calculate the thickness of a DNA / RNA target jet intersected by an incident projectile beam.

2. Theoretical description of a DNA / RNA base vapor jet

2.1. Equilibrium vapor pressure and total flux

The oven system comprises a cylindrical reservoir with a capillary exit to produce a jet with high directivity (see section 3). As the orifice cross section is ~1% of the reservoir cross section, the rate at which molecules *escape* through the capillary is very low compared to the frequency of collisions with the oven walls. Therefore, at a temperature T, the evaporative system reaches an equilibrium state characterized by a vapor pressure P_e which is close to the saturation pressure P_s. In these conditions, the thermodynamic properties of the vapor flow can be described using the Knudsen [6] method based on the kinetic theory of rarefied gas valid at equilibrium pressures < 10 Pa. Accordingly, in a closed container with a gas pressure P_s, the flow of molecules per unit area can be determined using the equation:

$$\frac{dN}{dt} = \frac{n\bar{v}}{4} \qquad \text{(eq. 1)}$$

where *n* is the number of molecules per unit volume and the velocity of the evaporated molecules is given by:

$$\bar{v} = \left(\frac{8 k_B T}{\pi m} \right)^{\frac{1}{2}} \qquad \text{(eq. 2)}$$

where k_B is the Boltzmann constant and *m* is the molecular mass. The vapor flow emerging from an ideal orifice of area A_0 can then be calculated as follows:

$$\frac{d\ N}{dt\ A_o} = \left(2\pi m k_B T\right)^{-1/2}\ P_e \qquad \text{(eq. 3)}$$

If we consider the capillary effect, the expression for the vapor flow must take into account the transmission probability given by the Clausing factor C of the tube capillary [7, 8]. At a given temperature, the equilibrium vapor pressure can then be determined indirectly by measuring the total mass flow from the oven.

Vapor pressure and consequently temperature are the key parameters for the study of jet properties. Accordingly, we can distinguish three flow regimes characterized by the Knudsen number $K_n = \lambda_0/L$ which is related to the capillary tube dimensions (L, d) and the molecular mean free path λ_0 as follows:

$$\lambda_0 = \frac{1}{\sqrt{2}\,\pi\sigma^2}.\frac{k_B T}{P_e} \qquad \text{(eq. 4)}$$

where σ is the effective diameter of the molecule (~ 6 - 7 Å for a DNA / RNA base [9]); $\pi\sigma^2$ represents the collision cross section for the given DNA/RNA base molecule.

- The molecular regime for $K_n > 10$ or $P_e \leq 0.26$ Pa, dominated by molecules traversing the capillary without intermolecular collisions
- The intermediate regime for $K_n > 0.1$ or $P_e \leq 100$ Pa
- The viscous regime for $K_n > 0.001$ or $100\ \text{Pa} \leq P_e \leq 2600$ Pa, dominated by intermolecular collisions along the capillary

The transition from molecular to viscous flow is defined as the intermediate regime with a mean free path which is similar to or smaller than the capillary dimensions: $\lambda_0 \leq d < L$. In this case, the flow is characterized by the competition between intermolecular collisions and collisions with the oven walls. The description of this regime is based on the introduction of an *effective length*:

$$L_{eff} = \sqrt{2\lambda L} \qquad \text{(eq. 5)}$$

Thus it is possible to take into account both the capillary dimensions and the molecular density. Following Troitskii's formula [9, 10], the angular distribution is given by:

$$\frac{d^2N}{d\Omega\, dt} = \frac{d^2N}{d\Omega\, dt}(0)\, \cos\theta^{\frac{3}{2}}\ f(u) \qquad \text{(eq. 6)} \qquad \theta \le \theta_0$$

$$\frac{d^2N}{d\Omega\, dt} = \frac{d^2N}{d\Omega\, dt}(0)\, \cos\theta^{\frac{3}{2}}\ f(\tau) \qquad \text{(eq. 7)} \qquad \theta \ge \theta_0$$

Where f(u) and $f(\tau)$ are error functions:

$$u = \frac{L}{L_{eff}\ \sqrt{\cos\theta}} \qquad \text{(eq. 8)}$$

$$\tau = \frac{d\ \sqrt{\cos\theta}}{L_{eff}\ \sin\theta} \qquad \text{(eq. 9)}$$

The original theoretical contribution of this work is to combine Troïtskii's [10] description of the angular distribution with the Knudsen [6] method for calculating the total flow.

3. Experimental methods

3.1. Total flow measurements

The gas-phase DNA / RNA bases which have been studied in the present experiments are uracil, adenine, thymine, and cytosine. Previous studies indicate that minimal thermal decomposition or isomerization of these DNA / RNA bases occurs between 375 and 475 K [11], thus we expected negligible effects in the temperature range 400-500 studied in the present work. Guanine, the remaining DNA base, was not studied in this work due to the reported difficulty of sublimating to a high vapor pressure without significant isomerization and / or thermal decomposition [12]. The DNA / RNA base powder samples were purchased from Sigma-Aldrich (minimum purity 99%).

The vapor jets studied were obtained by heating the DNA / RNA base powder in a custom-made oven. As mentioned above, this oven consists of a closed cylindrical powder reservoir (copper; internal diameter 10 mm) with a capillary exit (copper; length L = 35 mm, orifice diameter d = 1 mm). The reservoir cylinder was heated by a resistive filament ribbon and mounted in a ceramic outer casing for insulation. A thermocouple was inserted tightly in a hole in the base of the insulated reservoir cylinder. The DNA / RNA powder was heated progressively, with fine tuning of the heating power supply, until a stable sublimation temperature T was reached. The stabilization of the temperature was necessary to work in equilibrium state evaporation conditions. The DNA / RNA base vapor pressure was sufficiently high to form an intense neutral molecular beam at an oven temperature of 400 - 500 K.

The total vapor flux emerging from the capillary was determined indirectly by measuring the weight loss Δm of the oven for a given evaporated base powder during a time interval Δt. Figure 1 shows the system used to measure the mass flow from the oven at equilibrium temperature. The evaporated DNA bases were condensed onto a cold plate target during an exposure time of several hours. The evaporative system and the collecting target were mounted in a vacuum chamber maintained at approximately 10^{-6} mbar. Each deposit was carried out in stable temperature and steady-state evaporation conditions. The weight of deposit was deduced from the difference between the weights of the collecting plate target before and after vapor exposure.

Because of the limited acceptance of the collecting system, we have measured systematically the percentage of the collected weight relative to the initial powder weight in the oven. The mean value of this percentage was $\Psi = 69.4 \pm 1.6$ % (the uncertainty is the standard deviation of all the measurements).

3.2. Angular flux measurements

Knowledge of the angular distribution of the jet is essential in order to determine the target thickness in a crossed-beam experiment. In our previous study of a gas jet target [13] we have demonstrated that in the viscous flow regime the angular jet profile is independent of the pressure.

Similarly, the angular distribution depends only on the geometry of the capillary in the molecular flow regime [8, 10, 14-16]. In the case of intermediate flow (equations 6-9), however, the angular dependence is included in the error functions which depends on the effective length (L_{eff}). Therefore, it is necessary to study the effect of this angular dependence as a function of the oven temperature.

Figure 2 shows photographs corresponding to a thin and thick deposit of uracil obtained at the same sublimation temperature and for two exposure times, respectively 1h30 and 8 mn. The wavelength and order of interference rings visible in the photograph of the thin deposit are directly related to the thickness of condensed DNA / RNA bases. Thus the angular vapor flux pattern can be extracted from the optical profile. Photographs were taken with using CCD camera in order to store the interference pattern digitally. Using an image processing program developed in MATLAB, each tint was decomposed into its red, green, and blue (RGB) components so that pixels could be identified by a virtual matrix in the RGB space.

Figure 3 represents the intensity variation of the green (G) component along the interference ring diameter. Naturally, the interference is constructive if the optical path difference δ is an integer multiple of the wavelength λ (equation 10) and destructive if the path difference δ is a half-odd integer multiple of λ (equation 11).

$$\delta = 2ne(x) = k\lambda \qquad \text{(eq. 10)}$$

$$\delta = 2ne(x) = (2k+1)\lambda/2 \qquad \text{(eq. 11)}$$

where *n* represents the optical index and *e(x)* represents the local thickness.

In order to determine the wavelength of the G component used in the camera, the well-known black cross calibration method was applied. An interference pattern was generated using a spath plate mounted between two crossed polarizers. The precise wavelength of the camera G component could then be calculated by plotting the optical path difference induced by the spath plate against the interference order k. The linear fit gives a wavelength $\lambda(G)$ of 550.15 ± 0.15 nm.

4. Results and discussion

4.1. Total flow as a function of temperature

The measured mass deposition rates are plotted in Figure 4 as a function of the sublimation temperature T for the four DNA/or RNA bases studied. Two distinct regimes are identified for lower and higher temperature corresponding to molecular and viscous flow, respectively (see Table 1). According to Table 1, we can verify that a large part of our measurements are in the intermediate regime except the case of uracil molecules where the measurements concern the three flow regimes. Figure 5 presents the same data on a log-log scale. In the present conditions the thermo-dynamical properties of vapor flow are determined by the Knudsen method based on the kinetic theory of rarefied gas and applicable for equilibrium pressure $P_e < 0.1$ mbar.

$$P = \frac{D_t}{C A_o}\left(\frac{2\pi R T}{M_b}\right)^{1/2} \qquad \text{(eq. 12)}$$

Where A_0 is the surface area of the effusion orifice, C the Clausing coefficient of the capillary, T the temperature of the measurements, R the gas constant, M_b the molar mass of the nucleobase, and D_t = m/t (mass evaporation rate where m the mass of nucleobase sublimated over time t). Thus the present D_t(T) data has been used to determine the nucleobase temperatures which correspond to the vapor pressure ranges associated with molecular and viscous flow (Table 1). The present total mass flow measurements were carried out in the following temperature ranges: 390-454 K for thymine, 400-493 K for uracil, 414-452 K for adenine, and 428-478 K for cytosine. The Table 1 shows that these ranges correspond principally to the intermediate flow regime. However the uracil and thymine data also overlap with the viscous regime (above 471 and 446 K, respectively).

The molar enthalpy of sublimation ΔH_{sub} can be extracted from the vapor pressure and temperature using the Clausius-Clapeyron equations.

$$P(T) = A\exp\left(-\frac{\Delta H_{sub}}{RT}\right) \qquad \text{(eq. 13)}$$

where A is a constant.

Thus ΔH_{sub} was determined by generating a least-squares-fit to the Clausius-Clapeyron relation expressed in terms of the quantities measured in the present experiments:

$$Ln\left(D_t\, T^{1/2}\right) = Ln\left(\frac{C\, A_o\, M_b^{1/2}}{2\pi\, R}\right) - \frac{\Delta H_{sub}}{R\, T} \qquad \text{(eq. 14)}$$

Table 2 compares the present ΔH_{sub} (based on the absolute mass measurements, AMM) for uracil, cytosine, thymine, and adenine with previous values determined using
caloric (C), gas saturation (GS), Langmuir vaporization (LE), Mass Effusion (ME), Quartz Resonator (QR), Head Space Analysis (HSA), and Torsion Effusion (TE) methods. The uncertainties are also derived from the least-squares-fit and are mainly due to the experimental method of determination of the evaporated mass rate D_t. The agreement of our measurements with available data is a validation test for our method of extracting vapor pressure from the mass loss rate D_t using the Knudsen method.

4.2. Target thickness determination from theoretical profiles

In order to determine the absolute target thickness and thus derive absolute cross sections in a crossed beam experiment, both total and local vapor flux measurements are required. The target thickness ε at temperature T is given by the integral density n(x,y,z) over the incident beam - vapor jet overlap distance (x):

$$\varepsilon(T, y) = \int n(x, y, 0) I(x, y, z) dx \qquad \text{(eq. 15)}$$

where I(x,y,z) is the normalized beam profile which is assumed to be Gaussian, or uniform when the width of the incident beam is smaller than that of the vapor jet. Figure 6 shows a schematic view of the geometrical parameters used to define the vapor jet and thence derive its thickness along the trajectory of an incident beam. The flux density is the number of molecules entering the elementary surface dS per second at a given position.

$$dS = r^2\, d\Omega$$

$$\vec{j}(r,\theta,\varphi) = \frac{d^2N}{dS\,dt}\frac{\vec{r}}{r} = n(r,\theta,\varphi)\vec{v} \qquad \text{(eq. 16)}$$

$n(r,\theta,\varphi)$ is the density of vapor molecules (number of molecules per unit volume dr.dS) and $\vec{v}$ is the molecular velocity (equation 2).

In order to obtain a high target thickness in recent proton impact experiments using the present oven system [3, 35], the incident beam axis was located at a similar distance (y ~ 1 mm) above the capillary to the diameter of the orifice. Taking into account the results of the total flux measurements and the angular distributions, the target density can be approximated by the combination of a uniform density directly above the capillary orifice (cross sectional area A_0) with the angular distribution law of intermediate regime flow (equation 7).

4.3. Target thickness determination from the optical interference profile

As mentioned above, the present measurements concern two complementary parameters: the total flux $(dN/dt)_{total}$ and the angular flux $(dN/d\Omega\,dt)$. The total flux is determined by measuring the oven weight loss Δm during the time Δt by weighing the target plate before and after exposure to vapor. The angular flux distribution and consequently the density n(R,φ,z) are expressed in cylindrical coordinates. Consider an elementary surface ($dS = dRd\varphi$) of the interference pattern (Figure 6), where $j(R)$ denotes the vapor flux density. The number of molecules deposited on this surface element, dN_d, is given by:

$$dN_d = j(R)\,\Delta t\; R\,dR\,d\varphi \qquad \text{(eq. 17)}$$

This can be also expressed as a function of the deposit thickness e_d(R):

$$dN_d = \rho_d \frac{N_A}{M} e_d(R)\,R\,dR\,d\varphi \qquad \text{(eq. 18)}$$

Equations 17 and 18 express the linear dependence between the angular flux density and the deposit local thickness. The following expression can thus be deduced:

$$j(R) = K\ e(R) \qquad \text{(eq. 19)}$$

with $K = \rho_d \frac{N_A}{M}$ and $e(R) = e_d(R) / \Delta t$

The angular flux distribution is derived directly from the optical analysis of the interference rings. The total flow $(dN/dt)_{total}$ is determined from the measured mass deposition rate during steady-state evaporation.

$$\left(\frac{\Delta N}{\Delta t}\right) = \left(\frac{dN}{dt}\right)_d = \eta \left(\frac{dN}{dt}\right)_t \qquad \text{(eq. 20)}$$

where η is the geometrical factor related to the fraction of collected vapor compared to the total flowing from the capillary: η = 0.694 ± 0.014 (see section 3.1). The relation between the measured deposit D_t and the local thickness deposit e(R) for a given position R is given by:

$$\int_S j(R) 2\pi R\, dR = \int_s 2Ke(R)\pi R dR = \eta \frac{N_A}{M} D_t \qquad \text{(eq. 21)}$$

Thus equations 16 - 20 provide a complete description of the total flux deduced from D_t and the angular flux related to the optically measured local thickness e(R). Figure 7(a) shows the profile of the deposit thickness e(R) for uracil evaporated at ~425 K obtained by interference rings analysis (Section 3.2). Figure 7(b) shows the same profiles obtained by varying the sublimation temperature and normalizing to the maximum thickness. It should be noted that the width of the profile increases with the sublimation temperature. Indeed this behavior has been observed previously [14, 16, 36] in the intermediate regime. The comparison with the theoretical profiles demonstrates that this effect is related to the L_{eff} parameter and the competition between molecular and viscous flow.

Figures 8 and 9 include also theoretical profiles calculated using equations 6 and 7 for the present experimental conditions at various sublimation temperatures. In the upper part of Figure 8, both and

experimental and theoretical profiles are compared to the theoretical upper limit where intermolecular collisions in the capillary are neglected ($f(u) = 1$ and $f(\tau) = 1$). These profiles have been obtained when the capillary is at 26 mm from the deposit surface (see Figure 1).

The lower part of Figure 8 shows the experimental and the theoretical profiles F_0c when the error functions $f(u)$ and $f(\tau)$ are taken into account. The error function depends on the length and diameter of the capillary. The theoretical profiles IF_0c reported in the lower part of Figure 8 are obtained by integrating F_0c over the capillary dimensions in Cartesian coordinates. Naturally, the calculated upper limits of F_0 and IF_0 are equal in the upper and lower parts of the figure since F_0 does not depend on the capillary geometry. Figure 9 shows the same results plotted for six uracil sublimation temperatures corresponding to the intermediate flow regime.

The experimental results and the theoretical model are in good agreement both quantitatively and qualitatively. The dependence on the temperature is also described well. This indicates that the analytical expression of the theoretical model used in this study can be applied for absolute determination of both the total flux and angular distribution of DNA / RNA base jets with good accuracy.

6. Conclusion.

The DNA – base vapor-jet has been studied in the intermediate flow regime, corresponding to Knudsen number 0, $1 < K_n < 10$. The heat of the oven containing DNA – base powder has been adjusted in such manner to obtain stationary flow for all the studied temperature intervals. At a given temperature the corresponding pressure is determined assuming Knudsen hypothesis and knowing the transmission probability of associated capillary Clausing factor. This allows to relate temperature and pressure to total flux which is directly measured by a weighing method of the evaporated base powder quantity. The absolute flux density depending on the angular distribution of vapor molecules has been also studied experimentally using a method of optical interference. The measured profiles are in good agreement with analytical law given by Troïtskii in the intermediate regime, taking into account both

$(\cos\theta)^{3/2}$ angular dependence and the error function dependence on the free path of vapor molecule collisions. The absolute target thickness of the jet could be extracted with an accuracy of 10% resulting mainly from errors in the relative positions of the beam axes.

REFERENCES

[1] Y. Zheng, D.J. Hunting, P. Ayotte, and L. Sanche, Phys. Rev. Lett. 100 (2008) 198101.

[2] M. Dingfelder, M. Inokuti, and H.G. Paretzke, Radiation Physics and Chemistry 59 (2000) 255.

[3] B. Coupier, B. Farizon, M. Farizon, M. J. Gaillard, F. Gobet, N.V. de Castro Faria, G. Jalbert, S. Ouaskit, M. Carré, B. Gstir, G. Hanel, S. Denifl, L. Feketeova, P. Scheier, and T.D. Märk, Eur. Phys. J. D 20 (2002) 459.

[4] G. Hanel, B. Gstir, S. Denifl, P. Scheier, M. Probst, B. Farizon, M. Farizon, E. Illenberger, and T.D. Mark, Phys. Rev. Lett. 90 (2003) 188104.

[5] J. de Vries, R. Hoekstra, R. Morgenstern, and T. Schlathölter, Physica Scripta T110 (2004) 336.

[6] M. Knudsen, Ann. Phys. 28 (1909) 999.

[7] a) P. Clausing, J. Vac. Sci. Technol. 8 (1971) 636

b) P. Clausing, Physica 9 (1929) 65.

[8] D.J. Santeler, J. Vac. Sci. Technol. A 4 (1986) 338.

[9] S.K. Lilov, Cryst. Res. Technol. 21 (1986) 1299.

[10] V.S. Troïtskii, Sov. Phys. JETP 7 (1962) 353.

[11] C. Desfrançois, H. Abdoul-Carime, and J.P. Schermann, J. Chem. Phys. Rapid communications 104 (1996) 1792.

[12] V. Periquet, A. Moreau, S. Carles, J.P. Schermann, and C. Desfrançois, Journal of Electron Spectroscopy and Related Phenomena 106 (2000) 141.

[13] B. Farizon, M. Farizon, M.J. Gaillard, E. Gerlic, and S. Ouaskit, Nuc. Instrum. and Meth. in Phys. Res. B 101 (1995) 287.

[14] K. Wohrer, M. Chabot, R. Fosse, and D. Gardès, Rev. Sci. Instrum. 71 (2000) 2025.

[15] W. Steckelmacher, Rep. Prog. Phys. 49 (1986) 1083.

[16] C.A. Flory and S. Cutler, J. Appl. Phys. 73 (1993) 1561.

[17] J.S. Chickos and W.E. Acree, J. Phys. Chem. Ref. Data 31 (2002) 537.

[18] A.L.F. de Barros, A. Medina, F. Zappa, J.M. Pereira, E. Bessa, M.H.P. Martins, L.F.S. Coelho , W. Wolff, and N.V. de Castro Faria, Nucl. Ins. and Methods in Phys. Res. A 560 (2006) 219.

[19] B. Brunetti, G. Della Gatta, and V. Piacente, J. Chem. Eng. Data 45 (2000) 237.

[20] G. Bardi, L. Bencivenni, D. Ferro, B. Martini, C.S. Nunziante, and R. Teghil, Thermochim. Acta 40 (1980) 275.

[21] A.B. Teplitskii, I.K. Yanson, O.T. Glukhova, A. Zielenkiewicz, W. Zielenkiewicz, and K.L. Wierzchowski, Biophys. Chem. 11 (1980) 17.

[22] I.K. Yanson, A.B. Teplitskii, and L.F. Sukhodub, Biopolymers 18 (1979) 1149.

[23] M.J. Nowak, K. Szczepaniak, A. Barski, D. Shugar, Z. Natureforsch, and C. Biosci, 33C (1978) 876.

[24] M. Nabavian, R. Sabbah, R. Chastel, and M. Laffitte, J. Chim. Phys. Phys-Chi. Biol. 74 (1977) 115.

[25] I.K. Yanson, B.I. Verkin, O.I. Shlyarevskii, and A.B. Teplitskii, Stud. Biophys. 32 (1974) 29.

[26] B.C. Romanov, B.I. Sukkhorukov, E.A. Miroshnichenko, Yu. A. Lebedev, 1972, Fourth International Biophysical Congress, Abstract E7, (a4/7)b [quoted by Y.M. Fogel, V.A. Ankudinov, D.V. Pilipenko, and N.V. Topolia, Soviet Phys. JETP 7 (1958) 400.]

[27] L.B. Clark, G.G. Peschel, and I. Tinoco, J. Phys. Chem. 69 (1965) 3615.

[28] A. Zielenkiewicz, M. Wszelaka-Rylik, J. Poznanski, and W. Zielenkiewicz, J. Solution Chem. 27 (1998) 235.

[29] P.M. Burkinshaw and C.T. Mortimer, J. Chem. Soc. Dalton Trans. 1 (1984) 75.

[30] D. Ferro, L. Bencivenni, R. Teghil, and R. Mastromarino, Thermochim. Acta 42 (1980) 75.

[31] W. Zielenkiewicz, J. Chem. Eng. Data 45 (2000) 626.

[32] R.M. Stephenson and S. Malanowski, Handbook of the Thermodynamics of Organic Compounds, Elsevier, New York, 1987.

[33] A. Zielenkiewicz, W. Zielenkiewicz, L.F. Sukhodub, O.T. Glukhova, A.B. Teplitskii, and K.L. Wierzchowski, J. Solution Chem. 13 (1984) 757.

[34] J.D. Cox and G. Pilcher, Thermochemistry of Organic and Organometallic Compounds, Academic Press, New York, 1970.

[35] J. Tabet, S. Eden, S. Feil, H. Abdoul-Carime, B. Farizon, M. Farizon, S. Ouaskit, and T.D. Märk, *unpublished*

[36] W.G. Pollard and R.D. Present, Phys. Rev. 73 (1948) 762.

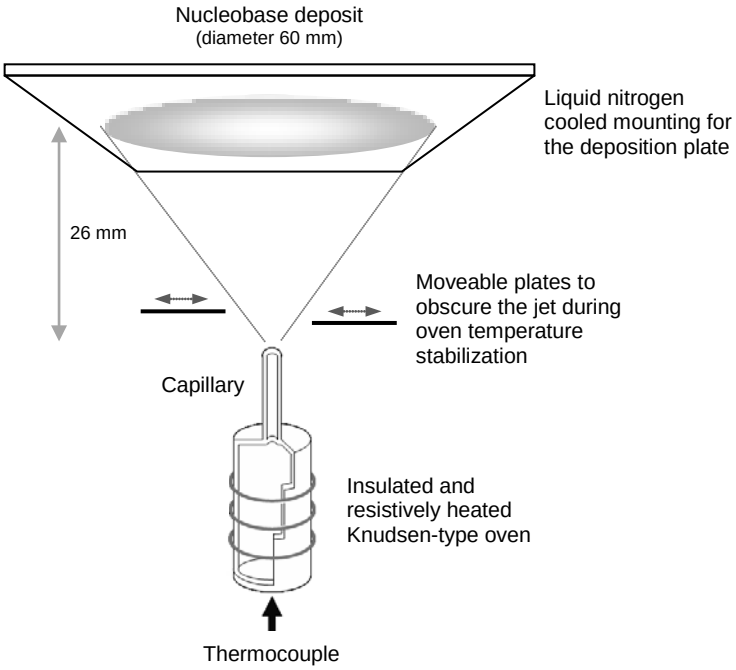

Figure 1: Schematic view of the DNA / RNA base vapor deposit set-up

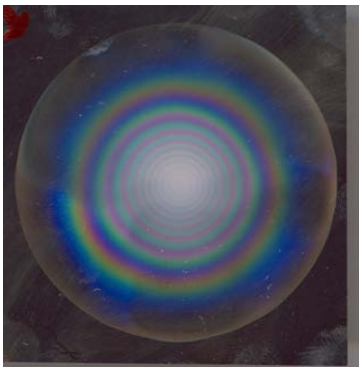

Thin deposit

Thick deposit

Figure 2: Photographs of a thin and a thick deposit of the uracil sublimated at ~ 433 K (respective exposure times: 1h30 and 8 h)

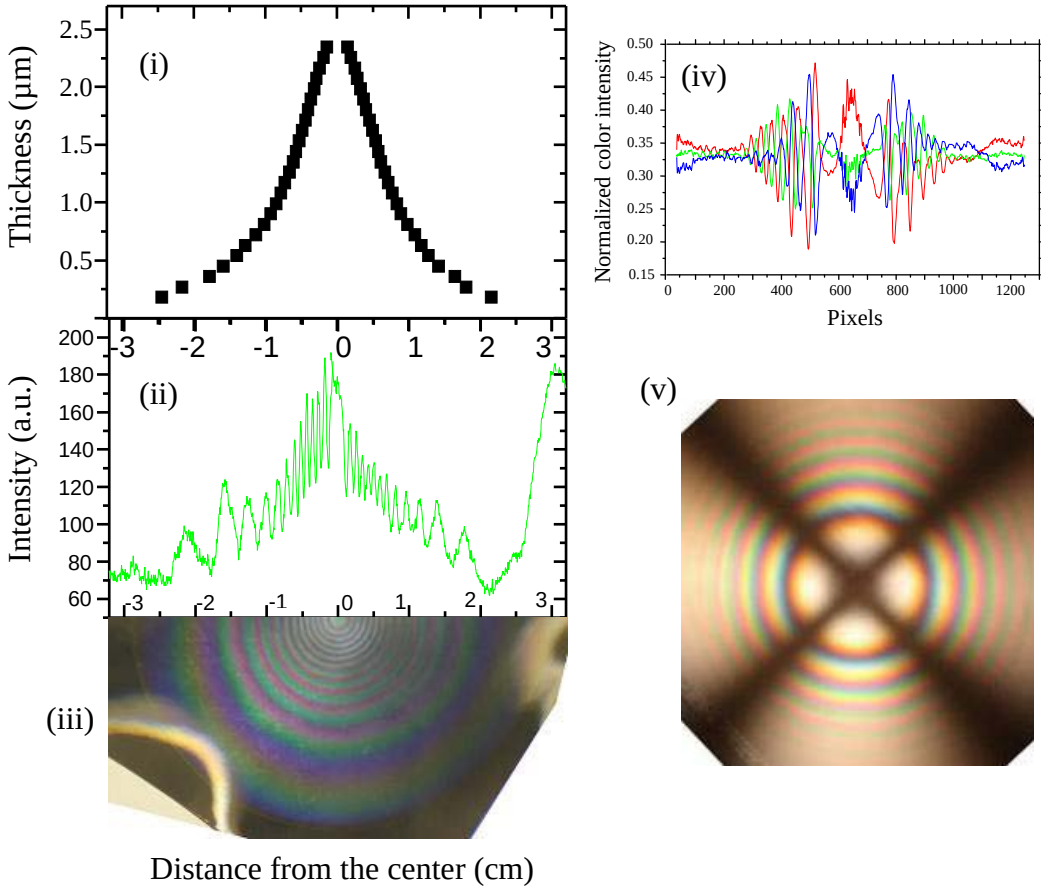

Figure 3: (i) Uracil deposit thickness profile derived from (ii) intensity measurements of the green (G) component of (iii) the photographed interference ring pattern

(iv) MATLAB analysis the color intensities (RGB) of (v) the “black cross” interference pattern generated using a spath plate between two crossed polarizers

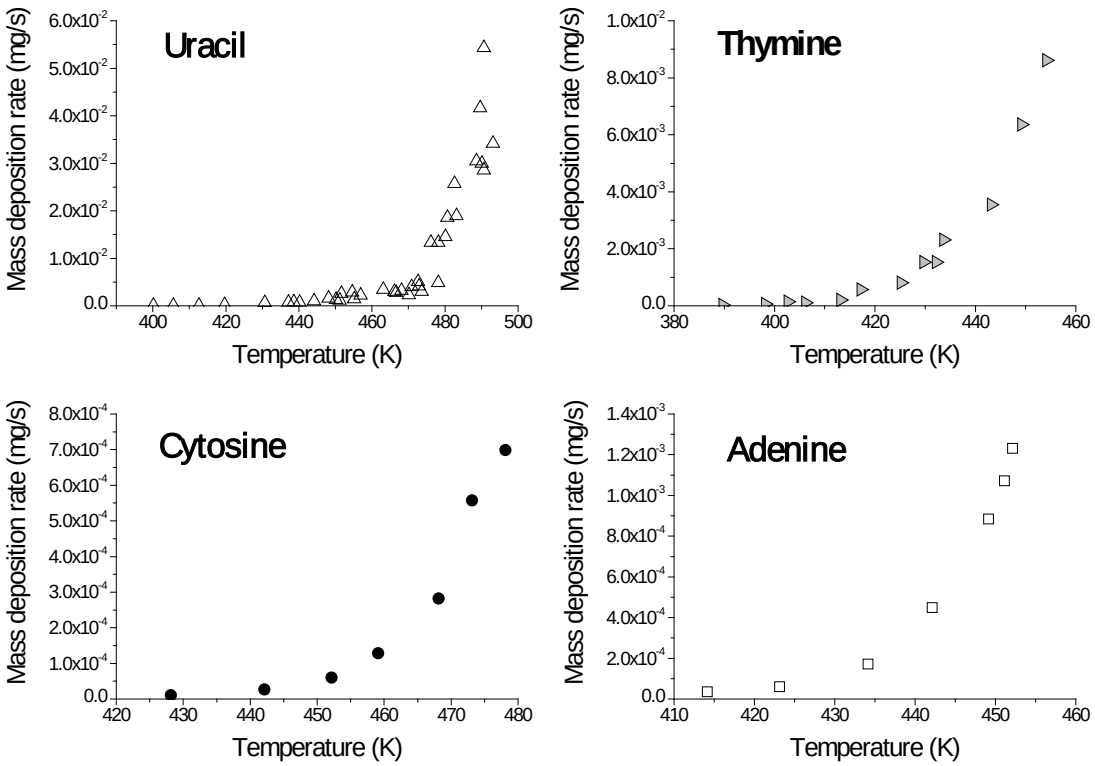

Figure 4: Mass deposition rates of DNA / RNA bases as a function of sublimation temperature

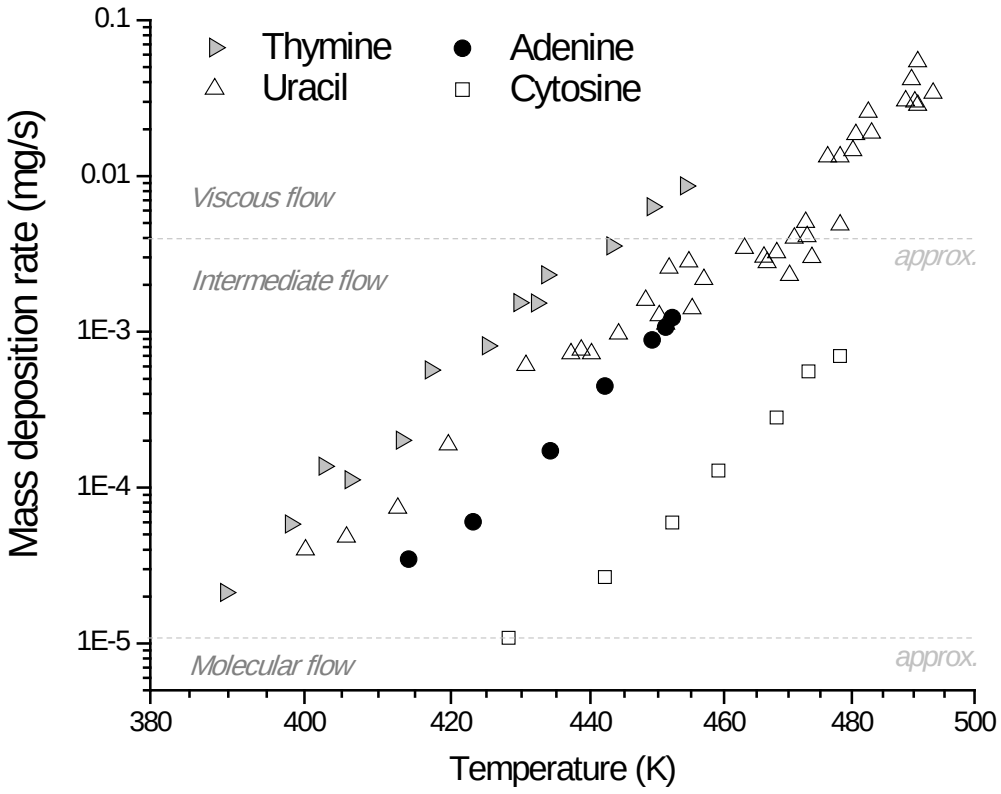

Figure 5: DNA / RNA base mass deposition rates plotted against sublimation temperature on a log-log scale. The dashed lines indicate the approximate boundaries between the flow regimes, as defined in Table 1.

Thymine = 390-454K = intermediate + overlap with viscous
Uracil = 400-493K = intermediate + overlap with viscous
Adenine = 414-452K = intermediate only
Cytosine = 428-478K = intermediate only

Flow regime	Uracil	Cytosine	Thymine	Adenine
Molecular regime $P_e \leq 0.26$ Pa	T < 391 K	T < 428 K	T < 388 K	T < 411 K
Intermediate regime $P_e \leq 100$ Pa	391 K < T< 471 K	428 K < T < 563 K	388 K < T < 446 K	411 K < T < 474 K
Viscous regime 100 Pa $\leq P_e \leq$ 2600 Pa	T > 471 K	T > 563 K	T > 446 K	T > 474 K

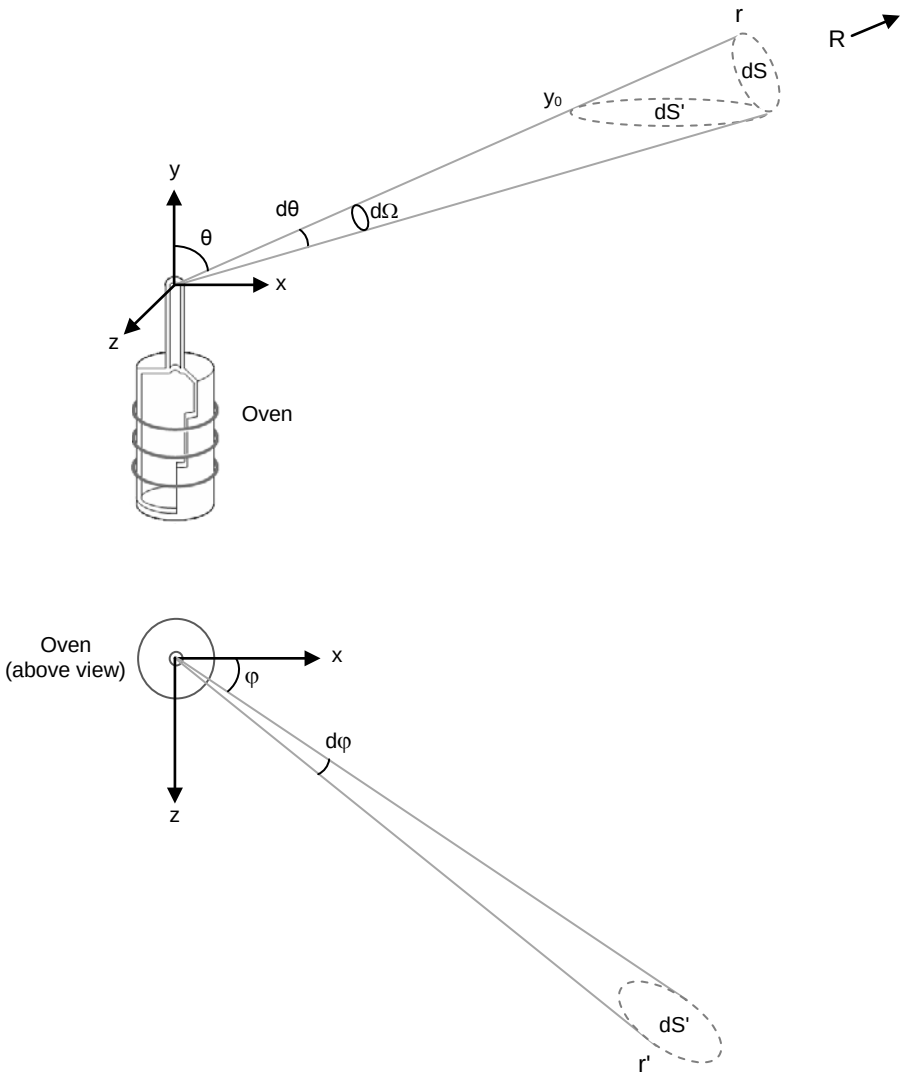

Figure 6: Schematic view of the oven showing the key geometrical parameters used to describe the nucleobase jet in equations 6-9, 15-18, and 21. The surface element dS at (r,θ,φ) from the capillary exit has normal direction R and solid angle dΩ. The surface element dS' and distance r' are projection onto the xz plane of dS and r, respectively.

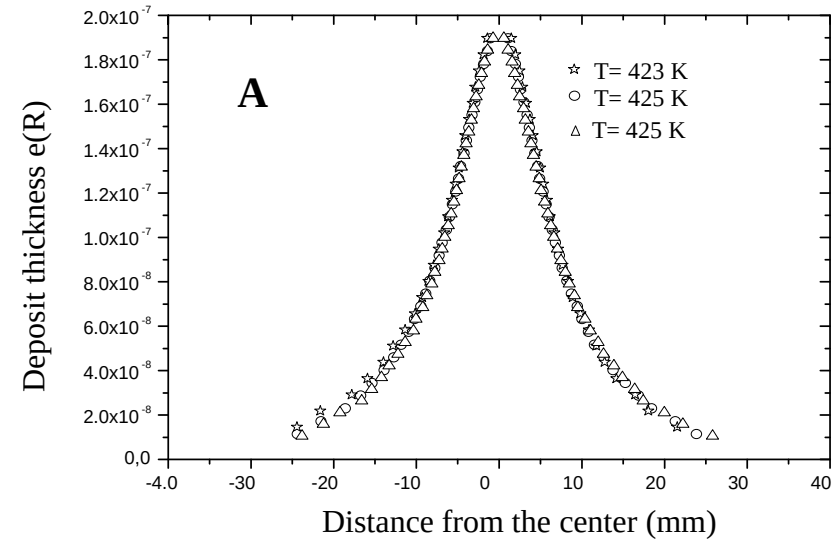

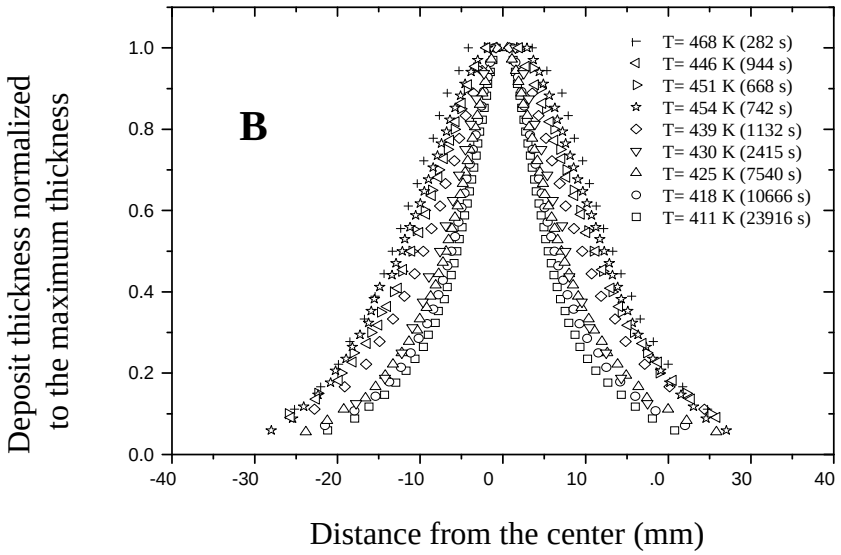

Figure 7

a) Uracil deposit thickness e(R) profiles (sublimation temperature ~ 425 K) obtained by interference pattern analysis

b) Experimental profiles obtained for different uracil sublimation temperatures and normalized to the maximum thickness

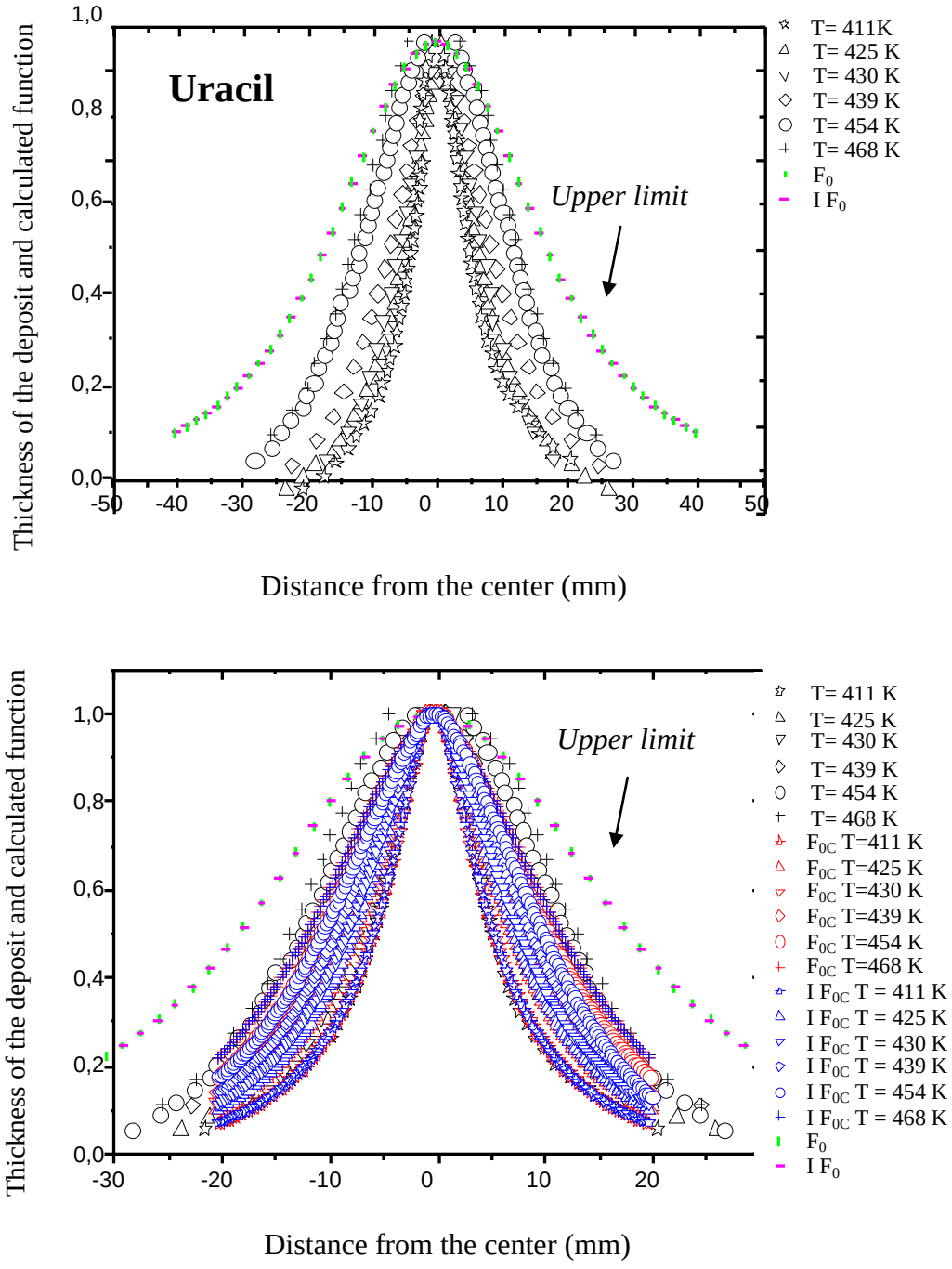

Figure 8: Comparison between theoretical and experimental profiles for various uracil sublimation temperatures. The theoretical profiles are calculated from equations 6 and 7 for the present experimental conditions (capillary 26 mm from the deposit surface, see Figure 1).

A: The experimental profiles are compared to the theoretical upper limits (IF_0) where the error functions f(u) and f(τ) are equal to 1 (i.e. intermolecular collisions in the capillary are neglected).

B: The experimental profiles are compared with the theoretical profiles IF_{0c}, taking into account f(u) and f(τ) for the present capillary dimensions.

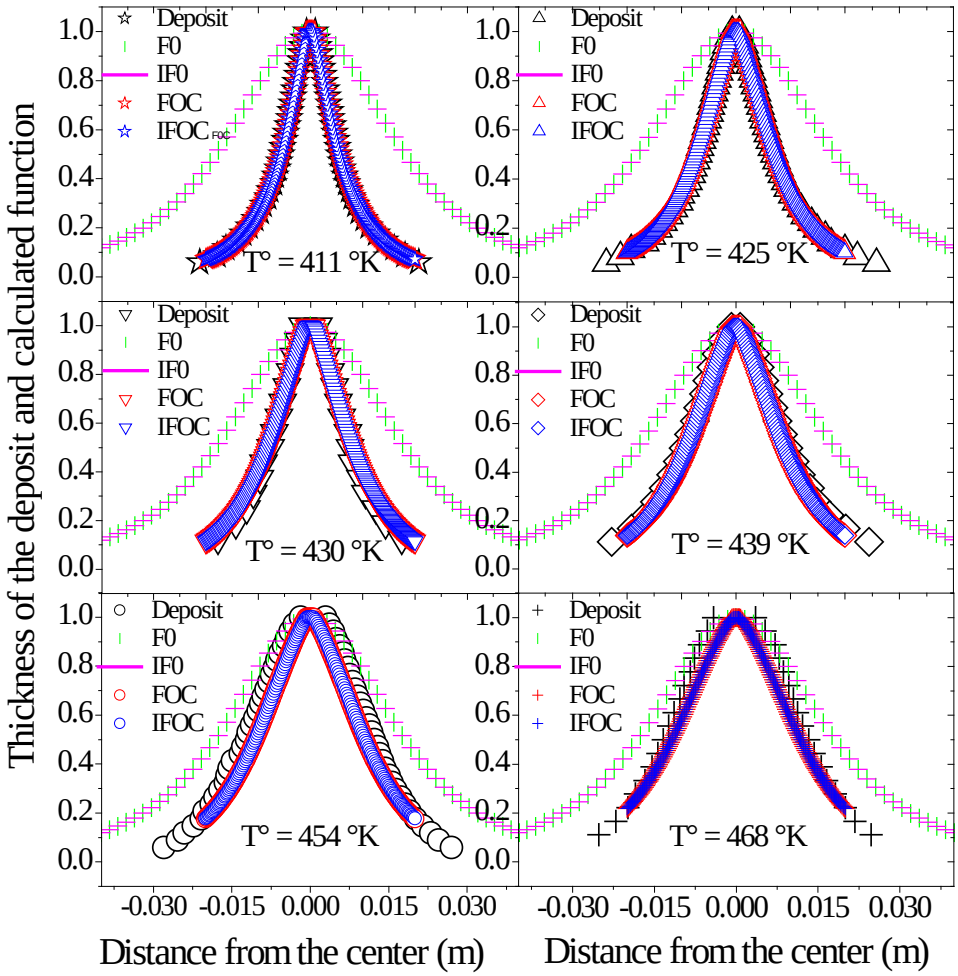

Figure 9: Comparison between theoretical and experimental profiles for each temperature of sublimated uracil.

Flow regime and pressure range (Pa)	**Temperature ranges (K) for each flow regime**			
	Uracil	**Cytosine**	**Thymine**	**Adenine**
Molecular regime $P_e \leq 0.26$	$T \leq 391$	$T \leq 428$	$T \leq 388$	$T \leq 411$
Intermediate regime $0.26 \leq P_e \leq 100$	$391 \leq T \leq 471$	$428 \leq T \leq 563$	$388 \leq T \leq 446$	$411 \leq T \leq 474$
Viscous regime $100 \leq P_e \leq 2600$	$T \geq 471$	$T \geq 563$	$T \geq 446$	$T \geq 474$

Table 1: The vapor pressure ranges for molecular, intermediate, and viscous regimes presented with the corresponding sublimation temperature ranges of DNA / RNA bases in a Knudsen-type oven

Nucleobase	$T_{min} - T_{max}$	ΔH_{sub} (kJ/mol)	T_m (°K)	Method	Reference
Uracil	**400 – 493**	**114,3 ± 5,8**	**–**	**AMM**	**Present results**
	315 – 435	125,3 ± 0,2	425	QR,ME	[18]
	394 – 494	127,0 ± 2	439	TE	[19]
	452 – 587	130,6 ± 4	519	ME,TE	[20]
	452 – 587	131 ± 5	298	TE,GS	[20]
	378 – 428	120,5 ± 1,3	403	QR	[21]
	–	121, 7	425	MS	[22]
	500 – 545	133,9 ± 8	523	HSA	[23]
	–	126,5 ± 2,2	440	C	[25]
	393 – 458	120,5 ± 5,2	426	LE	[26]
	–	115,5 ± 2,1	–	ME	[26]
	–	83,7	485	MS	[27]
Cytosine	**390 – 454**	**150,2 ± 8,3**	**–**	**AMM**	**Present results**
	320 – 410	167,7 ± 0,5	365	QR,ME	[18]
	505 – 525	151,7 ± 0,7	–	GS	[28]
	423 – 483	147,2 ± 2,6	453	ME	[29]
	–	155,0 ± 3	298	–	[29]
	–	167 ± 10	298	TE	[30]
	450 – 470	176 ± 10	298	C	[24]
Thymine	**414 – 452**	**141,6 ± 6,4**	**–**	**AMM**	**Present results**
	305 – 355	135,8 ± 0,4	330	QR,ME	[18]
	383 – 438	125,7 ± 3,6	411	ME	[29]
	–	131,3 ± 4	298	–	[29]
	378 – 428	124 ± 1,3	403	QR	[21]
	–	138 ± 10	298	TE	[30]
	–	134,1 ± 4,2	298	C	[24]
	–	124,3	–	LE	[25]
Adenine	**428 – 478**	**153,1 ± 6,9**	**–**	**AMM**	**Present results**
	305 – 360	130 ± 2	130	QR,ME	[18]
	400 – 438	140,4	–	ME	[31]
	448 – 473	109,2	460,5	–	[32]
	–	126,3	–	LE	[25]
	–	127,2	–	QR	[31, 33]
	–	108,7	–	ME	[27, 34]

Table 2: Enthalpy of sublimation for nucleobases: our results are compared to data compiled by Chikos and Acree [17].